

M agnetic and therm al properties of 4f/3d ladder-type m olecular com pounds

M . Evangelisti*

K am erlingh Onnes Laboratory, Leiden University, 2300 RA , Leiden, The Netherlands and
Instituto de Ciencia de M ateriales de A ragon, CSIC -Universidad de Zaragoza, 50009 Zaragoza, SpainM . L. Kahn^yLaboratoire des Sciences M oleculaires, Institut de Chim ie de la M atiere
Condensee de Bordeaux, UPR CNRS 9048, 33608 Pessac, France

J. Bartolom e

Instituto de Ciencia de M ateriales de A ragon, CSIC -Universidad de Zaragoza, 50009 Zaragoza, Spain

L. J. de Jongh

K am erlingh Onnes Laboratory, Leiden University, 2300 RA , Leiden, The Netherlands

C. M eyers, J. Leandri, and Y. Leroyer

Centre de Physique M oleculaire Optique et Hertzienne,
Universite Bordeaux 1, UMR CNRS 5798, 33405 Talence, France

C. M athoniere

Laboratoire des Sciences M oleculaires, Institut de Chim ie de la M atiere
Condensee de Bordeaux, UPR CNRS 9048, 33608 Pessac, France

(Dated: April 14, 2024)

We report on the low-tem perature m agnetic susceptibilities and speci c heats of the isostructural spin-ladder m olecular com plexes $L_2M(\text{pba})_3 \cdot x\text{DM SO}$, hereafter abbreviated with L_2M_3 (where $L = \text{La, Gd, Tb, Dy, Ho}$ and $M = \text{Cu, Zn}$). The results show that the Cu containing com plexes (with the exception of La_2Cu_3) undergo long-range m agnetic order at tem peratures below 2 K, and that for Gd_2Cu_3 this ordering is ferrom agnetic, whereas for Tb_2Cu_3 and Dy_2Cu_3 it is probably antiferrom agnetic. The susceptibilities and speci c heats of Tb_2Cu_3 and Dy_2Cu_3 above T_c have been explained by means of a m odel taking into account nearest as well as next-nearest neighbor m agnetic interactions. We show that the intraladder $L\{\text{Cu}$ interaction is the predom inant one and that it is ferrom agnetic for $L = \text{Gd, Tb}$ and Dy . For the cases of Tb, Dy and Ho containing com plexes, strong crystal eld e ects on the m agnetic and therm al properties have to be taken into account. The m agnetic coupling between the (ferrom agnetic) ladders is found to be very weak and is probably of dipolar origin.

PACS num bers: 75.30.-m ; 75.30.Gw ; 75.40.-s

I. INTRODUCTION

In today's search for sm aller, faster, m ore selective and e e cient products and processes, the engineering of well-de ned spatial m icroarrangem ents of pure and com posite m aterials is of vital im portance for the creation of new m agnetic devices. A possibility to assem ble m icrostructures in a controlled way is to use m olecular-based m aterials. The design of novel ferrom agnetic m olecular m aterials is certainly am ong the stimulating subjects.¹ In such a context, m olecular com plexes based on transition m etal ions are good candidates because the procedures for predicting the ferrom agnetic nature of the interaction in this class of m aterials have become fairly well established.^{2,3} However, such an understanding is much less advanced when a lanthanide ion is involved. M agnetic investigations concerning m olecular m aterials containing lanthanide and transition m etal ions have been overlooked until recently due to the weak interactions

present and the complications added by the orbital contribution of lanthanide ions.⁴ The case of Gd with a $^8S_{7/2}$ single-ion ground state and a quenched orbital contribution is special; most of the interest has been focused on the Gd{Cu combination because of the very frequently found ferrom agnetic character of the Gd{Cu interaction.^{5,6,7,8,9,10,11,12,13,14} Coupling those blocks in a 3D lattice would produce m olecular m agnets and possibly ferrom agnets.

In an extended polynuclear com plex, namely $\text{Gd}_2(\text{ox})[\text{Cu}(\text{pba})_3][\text{Cu}(\text{H}_2\text{O})_5] \cdot 20\text{H}_2\text{O}$ [hereafter abbreviated with $\text{Gd}_2\text{Cu}_3(\text{pba})$] with $\text{pba} = 1,3\text{-propylenediyl(oxamato)}$, not only the ferrom agnetic coupling of the Gd{Cu interaction was recently reported, but also the onset of a long-range m agnetic order.^{15,16} The crystal structure of this com pound consists of layers of double-sheet polymers separated by water m olecules. A puckered arrangement of $\text{Gd}[\text{Cu}(\text{pba})]$ units form s a two-dim ensional honeycom b pattern connected by oxalato groups. Discrete $[\text{Cu}(\text{H}_2\text{O})_5]^{2+}$ entities are

interspersed in the gap between the layers. From specific heat measurements, the onset of low-dimensional short-range order was found at temperatures around 1.5 K. By further lowering the temperature, the phase transition to three-dimensional ferromagnetic long-range ordering was observed at $T_C = 1.05$ K. This compound represents the first molecular-based ferromagnet involving lanthanide ions.

Although long-range ferromagnetic order has thus been found in Gd_2Cu_3 (pba), this material is isotropic due to the fact that both the Gd ions and the Cu ions are magnetically isotropic. A successful method to increase the intrinsic anisotropy is to synthesize intermetallic lanthanide (L) and transition metal (M) compounds, where the L has an orbital contribution, that introduces the anisotropy that the transition metal is lacking. Such a strategy has of course been applied in research on metallic ferromagnets, such as $Nd_2Fe_{14}B$. The strong orbit coupling within L, on one side, and the intense L-M exchange coupling has the net effect of polarizing the two sublattices in a direction, thus creating a strong uniaxial magnet, albeit, in a restricted temperature region.¹⁷ The same method in trying to increase the uniaxial anisotropy has been applied in a series of molecular compounds based on L and M ions, by choosing the L that induces such anisotropy (first condition), while expecting that the L-M interaction remains ferromagnetic and of similar intensity to that in the Gd_2Cu_3 (pba) compound (second condition). The L anisotropy of the ground state depends on the crystal field acting on the orbital moment.

In what follows, we shall describe the magnetic and thermal properties of a series of isostructural complexes based on lanthanide and transition metal ions. The general chemical formula of the compounds here studied is $L_2M(\text{opba})_3 \cdot x\text{DMF} \cdot y\text{H}_2\text{O}$ (hereafter abbreviated with L_2M_3) where $L = \text{La, Gd, Tb, Dy, Ho}$ and $M = \text{Cu, Zn}$, and opba stands for ortho-phenylenebis(oxamato), while DMF stands for dimethylsulfoxide. In view of previous work (Ref.¹⁸) proving that the L-Cu exchange for light L substitutions is antiferromagnetic, thus not fulfilling the second necessary condition above mentioned,

we have chosen to explore only the heavy L substitutions. Out of these, the most promising are the Tb and Dy substitutions, where there are already evidences of ferromagnetic coupling with Cu from susceptibility measurements, while no hint of such was found for Er, Tm or Yb.¹⁸ Recently, we have also reported, by means of specific heat experiments, the onset of long-range magnetically ordered states in the Tb and Dy substituted compounds.¹⁹ In this article we combine the thermal properties of L_2M_3 together with low-temperature susceptibility measurements, and explain the obtained results by means of theoretical calculations.

Another interesting property of this series of isostructural complexes is that they exhibit a spin-ladder structure. Spin-ladders are low-dimensional magnetic quantum systems that consist of two or more strongly magnetically coupled chains of spins and are thus intermedi-

ate between one and two dimensional magnetic systems. The magnetic properties of such systems have received a renewed experimental and theoretical interest since the discovery of high- T_C superconductivity in ladder structures provided by some cuprates like SrCu_2O_3 ,²⁰ or in vanadylpyrophosphate²¹ or in $\text{LaCuO}_{2.5}$.²² The research on novel molecular complexes with ladder geometries is a very important task for a better understanding of the physics behind these complex systems.²³

II. STRUCTURAL AND EXPERIMENTAL DETAILS

Information on the structure of the L_2M_3 series of compounds has been provided in detail in Refs.^{24,25}. Here, we summarize the most important information in view of the analysis of the magnetic properties given below.

The compounds crystallize very poorly and, consequently, a complete X-ray diffraction analysis could not be performed to determine the structure. Instead, the wide-angle X-ray scattering (WAXS) technique has been used to obtain structural information. Even though the WAXS technique cannot give the exact structure as compared to a full X-ray diffraction study, it has been successfully applied in several cases, for instance to structurally characterize inorganic polymers.²⁶ Furthermore, a complete structure determination by X-ray diffraction has been carried out on a related and very similar spin-ladder compound, namely, $\text{Tm}_2\text{Cu}(\text{opba})_3 \cdot x\text{DMF} \cdot y\text{H}_2\text{O}$ ($x = 10$; $y = 4$). This crystal structure has therefore been utilized as a starting point to interpret the WAXS data for the L_2M_3 compounds.

The analyses strongly suggested that the structure of L_2M_3 is likewise based on a discrete, infinite ladder-like motif, as shown in Fig. 1. The sidepieces of the ladder consist of $L_2M(\text{opba})_3$ units developing along the b direction with an alternation of L (III) and M (II) ions. Rungs provided by the precursor $M(\text{opba})_2^{2-}$, located between two L ions, connect the sidepieces. The L-M distance across an oxamato bridge is ≈ 5 Å, while the distance between two L ions across a M(opba) group is ≈ 11 Å. The shortest distance between two L ions (≈ 10 Å) involves non-connected L ions belonging to two sidepieces of neighboring ladders.

Each L ion is surrounded by seven oxygen ions, six of which belong to three opba ligands and one to a water molecule. The L coordination polyhedrons may be described as capped trigonal antiprisms. All the compounds are highly solvated with DMF and H_2O molecules, and the exact number of noncoordinated solvent molecules is not known accurately. Some of these molecules are easily removed. Therefore, there is some uncertainty in the molecular weight of the compounds and consequently in the absolute value of the molar susceptibility and specific heat.

The experiments done in the course of this work consisted primarily in measurements of three quantities:

magnetic susceptibility, magnetic moment and specific heat. Magnetic moment and susceptibility data down to 1.7 K were obtained with a commercial SQUID-based magnetometer with an ac-option. The ac-susceptibility of Gd_2Cu_3 in the temperature range $0.1 K < T < 3 K$ was measured in Zaragoza with a mutual inductance technique in a dilution refrigerator. The excitation amplitude was 10 mOe and the frequency $f = 160$ Hz. The signal was measured by means of a low-impedance ac-bridge, in which a SQUID was employed as a null detector.²⁷ The low-temperature susceptibilities down to 5 mK of Tb_2Cu_3 , Dy_2Cu_3 and Ho_2Cu_3 were measured in Leiden with an ac-susceptometer directly mounted inside the mixing chamber of a dilution refrigerator. The frequency of the experiments was $f = 520$ Hz. The data in the overlap region between 1.70 K and 3 K were used to convert the low-temperature data from arbitrary into absolute units. The specific heat measurements on $GdCu_3$, Gd_2Zn_3 and Dy_2Cu_3 in the range $0.2 K < T < 5.7 K$ were performed in Zaragoza by using an adiabatic calorimeter cooled by adiabatic demagnetization, using the heat-pulse technique and GEM thermometry. The error on the specific heat has been estimated to be less than 5%.²⁸ The specific heats of Tb_2Cu_3 , Ho_2Cu_3 and Ho_2Zn_3 were measured down to 0.1 K in Leiden using a thermal relaxation technique. The calorimeter was mounted in a dilution refrigerator and connected to a cold sink through a calibrated heat link. All data were collected on powdered samples of the compounds.

III. MAGNETIC PROPERTIES ABOVE 2 K

Magnetic properties of systems containing lanthanide ions, such as L_2M_3 , are significantly influenced by the interaction between a lanthanide ion and the surrounding ions in its direct environment. As a result, when a free lanthanide ion is placed in a crystal, its $2J+1$ fold degeneracy is partially lifted through electrostatic interaction between its f -electrons and the charges of the surrounding ions. The multiplet is split into a number of states, which can appropriately be termed the crystal field (CF) states. Magnetic susceptibility measurements may offer valuable information on the CF splittings. In this section we shall first present ac-susceptibility data above 2 K of La_2Cu_3 , Gd_2Cu_3 and Gd_2Zn_3 for which the CF effects can be neglected. Thereafter we shall briefly review and re-analyze in terms of the CF formalism the dc-susceptibility measurements on L_2M_3 , with $L = Tb$, Dy , Ho and $M = Cu$, Zn , which already appeared in Ref.¹⁸.

The ac-susceptibility of Gd_2Cu_3 was measured with a frequency of 90 Hz and an amplitude of 4 Oe of the exciting field. The dc-measurements of Ref.¹⁸ were performed in the temperature range $2\{300 K$, with a magnetic field of 10^3 Oe. Diamagnetic corrections of the constituent atoms were estimated from Pascal's constants as $291 \cdot 10^{-6}$ emu/mol. Due to the above mentioned un-

certainty in the molecular weights, it was assumed that for each compound the maximum expected value for the Curie constant was reached at 300 K, and the experimental data were rescaled accordingly when necessary.

Hereafter we use the notation J , J^0 and J^0 for the exchange constants of the $L\{Cu$, $Cu\{Cu$ and $L\{L$ interactions, respectively (negative values stand for antiferromagnetic interactions).

A. La_2Cu_3 , Gd_2Cu_3 and Gd_2Zn_3

The magnetism of La_2Cu_3 , where the lanthanide ion is diamagnetic, allows an estimate of the underlying $Cu\{Cu$ interaction. The single-ion magnetic properties of $Cu(II)$ are fairly straightforward. Spin-orbit coupling causes the g values of the lowest Kramers doublet ($S = 1/2$) to lie in the range 2.0 to 2.3. Figure 2 shows the data of La_2Cu_3 , which can be fitted to a Curie-Weiss law with $\theta = 0.2 K$. This suggests that, even though the distances in the ladder between next-nearest copper ions are as long as $\sim 10 \text{ \AA}$, they still interact with each other with a weak antiferromagnetic superexchange coupling. Taking $S = 1/2$, $\theta = 0.2 K$ and $z = 4$ for the number of nearest neighbors for each copper ion, the mean-field expression for the Curie-Weiss temperature²⁹ provides the value of $J^0 = k_B \theta = 0.2 K$ for this $Cu\{Cu$ interaction.

Gadolinium (III) has a $^8S_{7/2}$ ground state; the orbital contribution is almost entirely quenched and very isotropic g values close to the free electron value are found. For temperatures above 2 K, the in-phase ac-susceptibility of Gd_2Cu_3 follows a Curie-Weiss law with $\theta = 2.3 K$ and $C = 16.4 \text{ emu K mol}^{-1}$, indicating the ferromagnetic nature of the compound (Fig. 2). In the limit $T \rightarrow 0$, the paramagnetic susceptibility can be described by

$$\chi = \frac{C}{T} = \frac{2C_{Gd} + 3C_{Cu}}{T}; \quad (3.1)$$

where $C_{Gd} = N \mu_{eff}^2 (Gd) = 3k_B$ is the Curie constant of the two gadolinium ions and $C_{Cu} = N \mu_{eff}^2 (Cu) = 3k_B$ is the Curie constant of the three copper ions. Taking $S_{Gd} = 7/2$, $S_{Cu} = 1/2$ and $g_{Gd} = g_{Cu} = 2.00$, one obtains

$$C = 2C_{Gd} + 3C_{Cu} = 16.8 \text{ emu K mol}^{-1}$$

which is in satisfactory agreement with the experimental value ($16.4 \text{ emu K mol}^{-1}$). The same mean-field analysis used above gives the value of $J = k_B \theta = 0.5 K$ for the $Gd\{Cu$ exchange coupling. The origin of the ferromagnetic nature of the $Gd\{Cu$ interaction is further discussed in Section V A.

When the copper in Gd_2Cu_3 is substituted by diamagnetic Zn, then the susceptibility of Gd_2Zn_3 could be expected to follow the Curie law for two isolated Gd ions. Nevertheless, Fig. 2 shows that the Curie behavior (with

the expected value of $C = 15.7 \text{ emu K mol}^{-1}$) is no longer maintained below 10 K, since a slight decrease of the CT product from 15.7 down to 14.8 emu K mol^{-1} at 2 K is observed. The data are better described by a Curie-Weiss law with $\theta = 0.1 \text{ K}$. Such a deviation may be due to a weak, antiferromagnetic Gd-Gd interaction of dipolar origin. Since the Gd moment is large, dipole-dipole interactions could show up in the susceptibility at temperatures as high as 10 K, given the nearest-neighbor Gd-Gd distance of 10 Å. Of course it may also be attributed to a weak antiferromagnetic superexchange coupling acting between the Gd ions. The mean-field analysis provides the value of $J^{\text{eff}} = k_B = 6 \cdot 10^3 \text{ K}$ for this interaction, on basis of the obtained θ -value.

B. Tb_2Zn_3 , Dy_2Zn_3 and Ho_2Zn_3

As mentioned, for a lanthanide ion with a non-zero orbital moment, such as Tb, Dy or Ho, the effect of the crystal field on the magnetic levels has to be taken into account. In order to study the CF splittings for L_2M_3 , we consider the susceptibility measurements for the $\text{M} = \text{Zn}$ compounds to avoid (or reduce) the complication of magnetic exchange interactions. To simplify the analysis we consider the lanthanide ions in a cubic geometry, so that the number of crystal field parameters is minimized. As a further simplification, we consider an octahedral coordination for each lanthanide ion instead of the seven coordination found for $\text{Tm}_2[\text{Cu}(\text{opba})_3] \cdot x\text{DMF} \cdot y\text{H}_2\text{O}$ ($x = 10$; $y = 4$), which crystallizes in orthorhombic geometry.^{24,25} Although these simplifications may seem somewhat unsatisfactory, the lack of a precise knowledge of the actual coordination parameters (distances, angles) for the various L ions in L_2M_3 does actually not justify more sophisticated treatments. Within this approximation, the prediction of the type and the relative order of the CF split levels is greatly simplified. We use the valuable paper of Lea, Leask and Wolf²⁰ (hereafter referred to as LLW) which predicts both order and type of level in cubic symmetries for each value of the angular momentum and for all ratios of the crystal field parameters.

The crystal field acting on the lanthanide ion in octahedral geometry can be represented by the Hamiltonian

$$H_{\text{CF}} = B_4(O_4^0 + 5O_4^4) + B_6(O_6^0 - 21O_6^4); \quad (3.2)$$

where the O_n^m terms are angular momentum operators. The parameter B_n is related to the strength of the crystal field components

$$B_n = a_n A_n^0 \langle r^n \rangle;$$

where a_n is the operator equivalent factor, $\langle r^n \rangle$, for $n = 2, 4, 6$, respectively. A_n^0 are parameters relating the n th degree potential on the ion from the ionic charges of the lattice, and $\langle r^n \rangle$ are the expectation values for the distances of the 4f electrons. The product $A_n^0 \langle r^n \rangle$ is

determined to the first order by geometric factors and in principle can be calculated.

LLW have determined the eigenfunction and eigenvalue solutions for the Hamiltonian equation for applicable values of the angular momentum and the full range of B_4/B_6 ratios. They have constructed diagrams for the eigenvalues of the crystal field levels of each angular momentum in terms of a quantity x , defined as

$$\frac{x}{1 - x} = \frac{F(4)B_4}{F(6)B_6} = \frac{F(4)A_4^0 \langle r^4 \rangle}{F(6)A_6^0 \langle r^6 \rangle} = \frac{b_4}{b_6};$$

where $-1 < x < 1$, and $F(4)$ and $F(6)$ are multiplicative factors. Then, the susceptibility can be easily calculated for a given angular momentum and a gyromagnetic ratio. In the remainder of this section, we discuss the susceptibility data¹⁸ of L_2Zn_3 (with $\text{L} = \text{Tb, Dy, Ho}$) compounds and we explain them in terms of the LLW scheme. Only the temperature region below 40 K will be considered, since only the contribution of the lowest lying levels needs to be taken into account. These approximations are allowed in view of the large size of the level splittings compared to the low-temperature region of interest for our experiments (mainly below 10 K). This is confirmed by the specific heat analyses given below, where we shall show that only few CF levels are actually involved in the magnetic ordering processes.

Let us start with Tb_2Zn_3 . Compounds of non-Kramers lanthanide ions, such as Tb (III), often have a singlet electronic ground state separated by an energy from an excited singlet state. In a cubic field, the 7F_6 state of Tb is split into two singlets (ψ_1 and ψ_2), one non-magnetic doublet (ψ_3) and three triplets [ψ_4 , $\psi_5^{(1)}$ and $\psi_5^{(2)}$].

The measured susceptibility of Tb_2Zn_3 is shown in Fig. 3. The data at low temperatures are well described by two singlets split by $\theta = 0.2 \text{ K}$. In the LLW scheme for octahedral coordination, such a situation corresponds to $|x| = 0.45$ where the ground state can be either ψ_1 or ψ_2 (see Ref.³⁰). The assignment will be confirmed by the specific heat analysis presented below. For this simple case of two separated singlets, to improve the quality of the fit, we used ultimately a model in which a weak antiferromagnetic exchange interaction acting between the terbium ions has been taken into account. The fit provides the value of $J^{\text{eff}} = k_B = 1 \text{ K}$ for this interaction. The model used is explained in detail in the Appendix and employed in Section V B to explain the very-low-temperature magnetic and thermal properties of Tb_2Cu_3 .

For the case of dysprosium (III), the crystal field splits the $^6H_{15/2}$ ground state into two Kramers doublets (ψ_6 and ψ_7) and three quartets [$\psi_8^{(1)}$, $\psi_8^{(2)}$ and $\psi_8^{(3)}$] (see Ref.³⁰). In octahedral coordination with $|x| = 0.45$, as estimated for the previous case of Tb, one anticipates a doublet as the ground state (ψ_6 or ψ_7) with the higher state being the other doublet (ψ_7 or ψ_6 , respectively). The fit to the Dy_2Zn_3 data (Fig. 3) is in agreement with a low-lying doublet being either ψ_6 or ψ_7 separated by $\theta = 13.7 \text{ K}$ from ψ_7 or ψ_6 , respectively. Also this as-

signment will be confirmed by the analysis of the specific heat (see below).

Holmium (III) is a non-Kramers ion, with a 5I_8 ground state. The crystal field splits the ground state into one singlet (χ_1), two non-magnetic doublets [$\chi_3^{(1)}$ and $\chi_3^{(2)}$] and four triplets [$\chi_4^{(1)}$, $\chi_4^{(2)}$, $\chi_5^{(1)}$ and $\chi_5^{(2)}$]. The LLW diagram (see Ref.³⁰) is complicated, with many level crossings, which make simple choices difficult. For octahedral coordination with $\langle x^2 - y^2 \rangle = 0.45$, as in the Tb and Dy cases, one expects a $\chi_3^{(2)}$ ground state with $\chi_4^{(2)}$ the first excited state within a distance of not more than 20 K. The fit to the HoZn₃ data (Fig. 3) is in agreement with this, yielding the value of $\theta = 8.3$ K for the $\chi_3^{(2)} \{ \chi_4^{(2)}$ separation.

To summarize, the susceptibility data presented here for the Tb, Dy and Ho containing compounds, as well as the specific heat analyses presented below, can be reasonably accounted for by assuming cubic symmetry and octahedral coordination for the lanthanide ions. The consistency of the analyses is derived from the fact that the factor x could be taken at approximately the same value (0.45) for each compound. This is what one would expect for a series of isostructural compounds in which the lanthanide ions most probably have the same local coordination.

IV. VERY LOW-TEMPERATURE PROPERTIES

In the following sections, we present the thermal properties of the L_2M_3 compounds in the temperature range 0.1 to 10 K, and their magnetic properties down to 5 mK. We first analyze the lattice contributions to the measured heat capacities, and then describe the results inferred from susceptibility, magnetization and magnetic specific heat for each compound of the series.

A. Phonons contribution

Figure 4 shows the collected zero-field specific heat data of the L_2M_3 compounds as a function of temperature. As a first step, we have estimated the lattice contribution for each compound by fitting the high-temperature data to a sum of a Debye lattice contribution ($C_L = R = T^3$) and a high-temperature limiting tail ($\propto T^{-2}$) of the magnetic anomaly. The results for the parameter are given in Table I.

The WAXS analysis has shown that the L_2M_3 compounds have similar structures (see Section II and references therein). Consequently, one expects also a similar lattice contribution for each of them. Indeed, the estimated values for θ of the compounds studied fall into a fairly narrow range between $1.1 \cdot 10^2$ and $3.2 \cdot 10^2$ K³. Since the coefficient depends on the third power of the Debye temperature, such a limited variation appears quite acceptable. The only exception

is Dy₂Cu₃ for which $\theta = 8.8 \cdot 10^2$ K³, a value much higher than the others. The reason is presently not known. It is important to note that, however, the magnetic specific heat for Dy₂Cu₃ obtained after subtracting the phonon specific heat, appears to yield a magnetic entropy that agrees with the value expected for a doublet ground state.

The magnetic contributions to the specific heats of all the L_2M_3 compounds discussed in the following sections were obtained by subtracting the above mentioned lattice contributions.

B. Gd₂Cu₃ and Gd₂Zn₃

We have already seen (Section IIIA) that for temperatures above 2 K, the in-phase susceptibility of Gd₂Cu₃ follows a Curie-Weiss law with $\theta = 2.3$ K, indicating the ferromagnetic nature of the compound. The low-temperature in-phase susceptibility of Gd₂Cu₃ is depicted in Fig. 5 as a function of the temperature. A sharp peak is observed at $T_C = 1.78$ K which is probably due to a transition to long-range magnetic order. A large value of the susceptibility is found at the maximum (65.9 emu/mol). This behavior is typical for a powdered sample of an isotropic ferromagnetic material in which demagnetization effects become important. The theoretical value estimated for the susceptibility of a ferromagnetic sample of Gd₂Cu₃ at T_C is $\chi_{\text{ext}}^0(T_C) = N^{-1}$ (70–20) emu/mol, where N is the demagnetizing factor calculated taking into account an ellipsoidal approximation for the geometry of the sample. Within the error this is equal to the experimental result.

An interesting feature, that is discussed later (Section VA), is the in-phase susceptibility variation with the temperature for $T < T_C$ (Fig. 5). Just below T_C , the susceptibility goes through a minimum and further lowering the temperature reveals a rounded anomaly for $0.1 \text{ K} < T < 1 \text{ K}$.

Figure 6 shows the variation of the experimental magnetization M versus the field H for the temperature $T = 1.70$ K, i.e. just below the critical temperature ($T_C = 1.78$ K). No hysteresis effect is observed. Additional evidence for the ferromagnetic coupling is gained by comparison of the magnetization measurements to the calculated behavior for the uncoupled case. If the magnetic centers were all uncoupled, M would vary according to

$$M = 2N g_{\text{Gd}} B_{7/2}(g_{\text{Gd}}) + 3N g_{\text{Cu}} B_{1/2}(g_{\text{Cu}}) \quad (4.1)$$

where $B_{7/2}(g_{\text{Gd}})$ and $B_{1/2}(g_{\text{Cu}})$ are the Brillouin functions for Gd and Cu ions, respectively. The saturation magnetization would be given by

$$M = (2g_{\text{Gd}}S_{\text{Gd}} + 3g_{\text{Cu}}S_{\text{Cu}})N_B = 17N_B$$

The calculated magnetization for $T = 1.70$ K as derived from Eq. (4.1) is displayed in Fig. 6 together with

the experimental curve. It can be observed that the experimental data saturate at the predicted value and they lie above the expression of Eq. (4.1) in the whole temperature range. Such a behavior clearly indicates that the predominant interaction, i.e. the Gd{Cu interaction through the oxamate bridge, is ferromagnetic.

Let us now discuss the magnetic specific heat data by presenting first the result for the Gd_2Cu_3 compound (Fig. 7). A sharp increase appears when lowering the temperature below 1 K. Due to incomplete achievement of the ordering process in the temperature range of our experiments, an analysis of the experimental entropy is not possible.

Figure 8 shows the magnetic molar specific heat $C_m = R$ versus the temperature T for Gd_2Cu_3 . Two clear features can be observed: a distinct peak at $T_c = (1.78 \pm 0.02)$ K confirming the assignment of a long-range ordering process, and a rounded maximum around 0.8 K. We note that the rounded anomaly occurs in the same temperature range as that observed in the susceptibility experiments (Fig. 5). Figure 8 shows also that the magnetic contribution at $T > T_c$ is quite large and extends up to high temperatures, indicating the presence of important short-range ordering effects most probably related to the low dimensionality (no contributions from CF splittings are expected for Gd ions).

In order to calculate the entropy, we use the relation

$$S = R \int_0^{Z_1} (C_m(T) - R) dT; \quad (4.2)$$

together with the experimental values of C_m in the temperature range $0.2 \text{ K} < T < 5.7 \text{ K}$. For the extrapolation down to 0 K we assume a 3D ferromagnetic spin-wave type contribution ($\propto T^{3/2}$) and on the high-temperature side a T^{-2} dependence for C_m . The calculated entropy gives a value of $S = R \ln 2$. This corresponds to the maximum expected value ($= 3 \ln 2 + 2 \ln 8$) evidencing that both the Gd and Cu magnetic ions participate in the ordering process. As already said, the relatively large values of the specific heat above T_c may be associated with low-dimensional fluctuations within the ladders. This can be clearly seen by plotting the entropy variation as a function of the temperature (inset of Fig. 8). The calculated entropy variation above T_c gives $(S_1 - S_c) = 2.7 R \ln 2$, which is a rather large fraction in comparison with theoretical values of three-dimensional models of ferromagnets.³¹ All this agrees with the low-dimensional ladder-type magnetic structure of these materials.

C. Tb_2Cu_3

The low-temperature susceptibility of Tb_2Cu_3 is depicted in Fig. 9. The abrupt change of the in-phase susceptibility at 1 K is ascribed to a transition to a magnetically ordered state, which is obvious also from the spe-

cific heat curve shown in Fig. 10. The maximum value is 93.6 emu/mol at 1.0 K. This value is almost of the same order as expected for a ferromagnetic material in which demagnetization effects become important. In fact, an estimate of the demagnetizing factor gives the value of

280 emu/mol for the susceptibility of an isotropic ferromagnetic Tb_2Cu_3 sample at the maximum, assuming a cylindrical approximation of its shape. At the low temperature side of the anomaly, the susceptibility decreases sharply, reaching a value of 5.0 emu/mol at 10 mK. The specific heat data are plotted in Fig. 10 and indicate a transition temperature of $T_c = (0.81 \pm 0.01)$ K. In the susceptibility data we see that fluctuations in the ordering process show up as a peak in the out-of-phase susceptibility⁰⁰ centered at 0.7 K (inset of Fig. 9), whereas the in-phase susceptibility⁰ shows an inflection point (maximum in $\chi^0 = \chi(T)$) at that same temperature. The⁰⁰ is in arbitrary units because it is null above 0.8 K and, thus, it was not possible to scale to data measured above 1.7 K with the commercial magnetometer. The observed behavior is not uncommon for a low-dimensional system which undergoes a phase transition to long-range magnetic order, for instance to an antiferromagnetic arrangement of the ferromagnetic ladders, at $T_c = 0.81$ K as deduced from the inflection point of⁰. The relatively large value of the susceptibility at 1 K may suggest the presence of a dominating ferromagnetic interaction, probably associated with the intraladder Tb{Cu interaction. We will return to this point in Section V B. Moreover, the very low value reached by the in-phase susceptibility in the limit of very low temperature, clearly indicates the large anisotropy of the terbium ions in Tb_2Cu_3 , as already pointed out in Section III B for Tb_2Zn_3 . The anisotropy may also be responsible for the fact that the measured value of the⁰ at T_c is lower than the expected limit for an isotropic ferromagnetic sample. Since a powder is measured, the value is a directional average.

The main feature of the magnetic specific heat of Tb_2Cu_3 , depicted in Fig. 10, is the peak at $T_c = 0.81$ K indicating the transition to a long-range ordered state. The bump observed above T_c and centered around 1.5 K is probably associated with low-dimensional fluctuations within the ladders, since a contribution from excited CF-levels is not expected in this temperature range (see Section III B). The data at the low-temperature side show a slight upward curvature. Below 0.4 K, the data obey the law $C_m T^2 = R = 0.05 \text{ K}^2$. This contribution is probably coming from the hyperfine splitting of the magnetic levels of the Tb nuclei. Subtracting the calculated hyperfine specific heat from the measured specific heat data, we estimate the remaining entropy. In order to calculate the magnetic entropy of Tb_2Cu_3 , we carry out the integration in Eq. (4.2) using the experimental values of $C_m = R$ in the temperature range $0.1 \text{ K} < T < 5 \text{ K}$. After extrapolation down to 0 K with an exponential function, the calculated entropy gives a value of $S = R \ln 2$. Taking into account that Cu has spin 1/2, which corresponds to $S = R \ln 2$ per atom, the experimental entropy con-

tent indicates that Tb has an effective spin 1/2, corresponding to a lowest lying doublet in the temperature region of the magnetic ordering process. In Section IIIB we have shown that for Tb₂Zn₃ the lowest energy levels are two singlets with a separation of $\Delta = 0.2$ K. For Tb₂Cu₃ we expect a similar crystal environment and, as a consequence, a similar energy scheme. Nevertheless, the separation Δ is relatively small in comparison with the thermal energy in the region of the magnetic ordering process. We thus conclude that we can apply the approximation of effective spin 1/2 for the Tb ion. In agreement with the pronounced high-temperature specific heat tail observed in Fig. 10, only about 15% of the entropy is left below T_C . This is another indication of the large amount of short-range magnetic order that is probably associated with the low dimensionality of the ladder.

D. Dy₂Cu₃

Figure 11 shows the low-temperature ac-susceptibility of Dy₂Cu₃. As in the case of Tb₂Cu₃, and as evidenced from the specific heat experiment presented in Fig. 12, clear evidence of a transition to a magnetically ordered phase is found. The in-phase susceptibility has a sharp peak centered at 0.8 K with a maximum value of 116.4 emu/mol. Below the peak, it decreases very sharply and remains almost constant at 10.0 emu/mol down to 10 mK. As for Tb₂Cu₃, the maximum of the experimental susceptibility is not far below the expected theoretical limiting value ($\chi = 280$ emu/mol) for an isotropic ferromagnetic sample. The out-of-phase susceptibility also shows a sharp peak centered at 0.77 K and it is zero below 0.4 K and above 1 K (inset of Fig. 11). At 0.77 K an inflection point occurs in the temperature dependence of the χ' . The transition temperature deduced below from the specific heat is $T_C = (0.75 \pm 0.01)$ K. Similar as for Tb₂Cu₃, the data point toward a type of antiferromagnetic long-range ordering, with very small value for the antiferromagnetic coupling (J_{AF}) between the ferromagnetic ladders. Since for an antiferromagnet χ at T_C is inversely proportional to J_{AF} , when the latter becomes small enough, χ at T_C can reach the demagnetizing limit. It is then difficult to distinguish between ferro- or antiferromagnetic coupling between the ferromagnetic chains. The peak in the χ'' found in both compounds may be due to a weak-ferromagnetic moment which arises when the antiferromagnetic ordering is accompanied by some degree of spin canting. Again, as for Tb₂Cu₃, the very low value of the in-phase susceptibility for $T \rightarrow 0$ indicates large anisotropy of the Dy ions.

Figure 12 shows the magnetic specific heat, plotted as $C_m = R \ln \Omega$ versus T , for the Dy₂Cu₃ compound, where $C_m = R \ln \Omega$ is the molar specific heat and T is the temperature. The prominent spike below 1 K is identified with the anomaly indicating the onset of a phase transition to a long-range ordered state. The peak is very sharp and allows an accurate determination of the critical tem-

perature as $T_C = (0.75 \pm 0.01)$ K. The analysis of the magnetic entropy content shows that only a very small portion (about 15%) is obtained below T_C and that, as for Tb₂Cu₃, the lanthanide has an effective spin 1/2 in the ground state, once more agreeing with the crystal field analysis (Section IIIB).

E. Ho₂Cu₃ and Ho₂Zn₃

The low-temperature susceptibility of Ho₂Cu₃ is shown in Fig. 13. Also for this compound, evidence of an antiferromagnetic long-range ordering is observed. The in-phase susceptibility has a maximum of 27.5 emu/mol at 0.12 K (much lower than for Tb₂Cu₃ and Dy₂Cu₃). It sharply decreases down to 8.9 emu/mol at 30 mK, and remains nearly constant by further lowering the temperature down to 5 mK. The out-of-phase susceptibility shows a peak around 40(100) mK, in which temperature range also an inflection point, centered at (50 \pm 10) mK, is seen in the in-phase susceptibility.

The molar specific heat of Ho₂Cu₃ is depicted in Fig. 14 together with that of Ho₂Zn₃ for comparison. The specific heats of Ho₂Cu₃ and Ho₂Zn₃ are seen to overlap for $T > 0.8$ K, showing a broad rounded anomaly with a maximum at 3.5 K (Fig. 14). This is probably due to crystal field splitting of the holmium levels. In Section IIIB we have seen that the susceptibility of Ho₂Zn₃ down to 2 K may be explained in terms of a doublet ($\frac{2}{3}$) ground state separated by 8.3 K from a triplet ($\frac{2}{4}$) excited level. Taking into account a further splitting of these degenerate levels, the Schottky contribution arising from this configuration can be easily calculated. A nice agreement with the data is obtained for $\frac{2}{3}$ further split by 2 K, and separated by 11 K from $\frac{2}{4}$, further split by 5 K each level (Fig. 14).

For Ho₂Zn₃, a sharp increase of the specific heat by lowering the temperature is observed below 0.3 K. This contribution is apparently coming from the hyperfine splitting of the magnetic levels of the Ho nuclei. In this temperature region, by fitting the data to $C_m = R(aT^b)$, we obtain $a = 0.14$ and $b = 1.3$, and not the expected value of $b = 2$, for a magnetic anomaly high-temperature tail. The reason for that is probably related to problems of thermal contact between spin system and the lattice, since we found the specific heat at low temperature to become increasingly dependent on the measuring time we used in the experiments. In fact, both specific heats of Ho₂Cu₃ and Ho₂Zn₃ have been measured with the relaxation technique. If the measuring time is not long enough for the sample to achieve thermal equilibrium, between the spin system and the phonon bath, part of the electronic spin contribution will simply be missing. Also for Ho₂Cu₃ an upward curvature is observed by lowering the temperature below 0.7 K. By comparison with the Ho₂Zn₃ results, we see that in the specific heat of Ho₂Cu₃ there is an extra contribution besides

the hyperfine splitting of the Ho nuclei. This may readily be explained by a weak Ho{Cu coupling that, together with the dipole-dipole interladder interaction, shows up at very low temperature. Consequently, only the onset of a phase transition is observed. The low-temperature limit of our setup did not allow to determine the ordering temperature that has to be below 0.1 K (judging from the -data). In combination with the susceptibility results (Fig. 13), we conclude that the ordering temperature T_C for Ho_2Cu_3 is between 0.04 and 0.10 K.

Due to the incomplete achievement of the magnetic ordering processes at the lowest temperature, the analysis of the entropy contents for Ho_2Cu_3 and Ho_2Zn_3 is not possible.

V. COMPARISON WITH LADDER MODELS

A. Gd_2Zn_3 and Gd_2Cu_3

For Gd_2Zn_3 , the sharp increase of the specific heat below 1 K (Fig. 7) may reflect the onset of a 3D ordering process, which takes place at a temperature lower than obtained in the experiment. Even though the Gd_2Zn_3 compound is more poorly crystallized than the Cu-containing compounds,²⁵ its measured specific heat clearly underlines the relevance of the Gd{Cu interaction, when compared with the results found for Gd_2Cu_3 . The absence of the copper at M sites reduces or inhibits the ordering temperature of the Gd sublattice below our lowest experimental temperature. It is clear that the Cu ion in Gd_2Cu_3 is much more effective than the Zn ion in transmitting magnetic exchange interaction along the Gd-oxamato-Cu-oxamato-Gd superexchange pathway that gives rise to the net ferromagnetic coupling.

In order to explain the paramagnetic susceptibility of Gd_2Cu_3 , let us consider the model proposed by Georges et al.¹⁴ for ladder-type double chains which has been successfully applied to describe the paramagnetic susceptibility of the $\text{Gd}_2(\text{ox})[\text{Cu}(\text{pba})_2[\text{Cu}(\text{H}_2\text{O})_5]] \cdot 20\text{H}_2\text{O}$ compound. This model, which is based on the standard transfer matrix method, takes into account the presence of copper quantum spins and gadolinium classical spins, in a ladder-like arrangement similar to the L_2M_3 compounds, where each gadolinium ion interacts isotropically with two neighboring copper ions. The approximation is the classical treatment of the gadolinium spin, which is allowed because of the high spin value of the ion.

With the aid of this model, we have analyzed the experimental thermal dependence of the susceptibility in the paramagnetic regime. The same Landé factor $g = 2.00$, determined in the high-temperature limit, has been attributed to all cations. A unique coupling constant J has been introduced for all the Gd{Cu isotropic interactions. The best fitting of the experimental susceptibility results is obtained in the range $2.5 \text{ K} < T < 20 \text{ K}$. Figure 5 shows the calculated curve with $J = k_B = 0.74 \text{ K}$. As expected, the positive J value refers to a ferromagnetic

exchange coupling, in agreement with the positive paramagnetic Curie temperature $\theta = 2.3 \text{ K}$. It is worthwhile to note that the J value obtained here does not differ substantially from the estimate of 0.5 K given in Section IIIA deduced by simple mean-field analysis. At temperatures below 2.5 K, the three-dimensional ordering mechanism becomes apparent and, consequently, the experimental data can no longer be described with the above (paramagnetic) model.

It is well established that an array of isotropic spins with dimensionality two or less will not present long-range ordering.³¹ The experimental specific heat data have shown the presence of short-range order for temperatures far above T_C already, and we have associated it with extended magnetic correlations along the spin ladders. The observed long-range ordering at $T_C = 1.78 \text{ K}$ implies the existence of interactions between adjacent ladders. The structure of Gd_2Cu_3 does not present any pathway between adjacent ladders that involve atomic contacts suitable for the propagation of magnetic exchange. Consequently, it seems reasonable to assume that the driving force for the magnetic long-range order is indeed the dipolar interaction.

Another interesting feature in Gd_2Cu_3 is the maximum observed at about 0.8 K, and thus below $T_C = 1.78 \text{ K}$, in both the susceptibility (Fig. 5) and the specific heat (Fig. 8). To explain such a feature, we may consider the presence of two types of interchain coupled systems in Gd_2Cu_3 , e.g. with slightly different packing of the ladders within the crystal structure. Then one polytype has $T_C = 1.78 \text{ K}$ and the other has a lower critical temperature of 0.8 K. Unfortunately, due to the lack of a precise knowledge of the structure and to the fact that the experiments have been performed on powdered samples, a detailed study of the ordering process could not be carried out.

For the sake of completeness we wish to mention briefly the nature of the mechanism of the Gd{Cu interaction. In preceding works,^{12,13} the ferromagnetism of this interaction was attributed to the coupling between the $4f\{3d$ ground configuration and the excited configuration arising from the metal-metal charge transfer configurations. The latter is associated with the $3d \rightarrow 5d$ process: an electron is transferred from the singly-occupied orbital centered on copper toward an empty orbital centered on gadolinium. In such a mechanism, J is given by

$$J = \sum_{i=1}^X \left[\int_{5d}^2 \int_{3d}^2 = (4U^2 - \epsilon^2) \right]_{ii} \quad (5.1)$$

where $\int_{5d}^2 \int_{3d}^2$ is the transfer integral of the $3d \rightarrow 5d$ process, ϵ is the energy gap between $S = 3$ and $S = 4$ excited states arising from the $4f^7 5d^1$ electron-transfer configuration and U is the energy cost of such a transfer. The summation applies to the five $5d$ gadolinium orbitals.

It is interesting to compare, qualitatively, the here obtained coupling constants J of Gd_2Cu_3 ($J = k_B = 0.74 \text{ K}$)

and of $Gd_2(ox)[Cu(pba)_3][Cu(H_2O)_5] \cdot 20H_2O$, which is a long-range ordered ferromagnet for $T_C = 1.05$ K^{15,16} and has $J=k_B = 0.40$ K.¹⁴ The difference may in fact be understood on the basis of the above mechanism. In the latter compound, the Gd ions adopt a distorted capped square antiprism coordination of oxygen atoms; six out of a total of nine oxygen atoms are provided by the three bridging Cu(pba) groups, two by the oxalato ligand, and the last one by a water molecule.³² In the former compound, due to the absence of the oxalato ligand, the 5d orbitals of the gadolinium ions are distributed in a less distorted environment. This fact, together with slightly shorter Gd{Cu} distances for Gd_2Cu_3 (see Refs.²⁵ and³² for comparison), gives higher values of J_{5d-3d} for Gd_2Cu_3 . Consequently, according to Eq. (5.1), the coupling constant J should indeed be larger for Gd_2Cu_3 than for $Gd_2(ox)[Cu(pba)_3][Cu(H_2O)_5] \cdot 20H_2O$, as found.

B. Tb_2Cu_3 , Dy_2Cu_3 and Ho_2Cu_3

Our measurements show Tb_2Cu_3 , Dy_2Cu_3 and Ho_2Cu_3 to be strongly anisotropic systems with long-range order phase transitions below 1 K. As for Gd_2Cu_3 , the low-dimensional structure of the compounds implies that the driving force for the long-range magnetic order is the dipolar interaction between the ferromagnetic chains. However, for Tb_2Cu_3 and Dy_2Cu_3 , evidence for an even larger amount of short-range order, associated with fluctuations within the ladder structure, is found above T_C . From the specific heat data, we have deduced that Tb_2Cu_3 and Dy_2Cu_3 may be described in terms of an effective spin 1/2 at low temperatures. We note that an effective spin 1/2, arising from a low-lying doublet, is often found for lanthanide compounds of dysprosium and terbium with low magnetic ordering temperature.³³ At higher temperatures the behavior is strongly modified by the presence of low-lying excited states.

To explain the magnetic and thermal properties of Tb_2Cu_3 and Dy_2Cu_3 , a model has been developed, which is based on the standard transfer matrix technique, using the Ising approximation and assuming spin 1/2 for the L and the Cu ions. The details of the model can be found in the Appendix. As revealed from the susceptibility measurements, we have to expect a ferromagnetic coupling J for the L{Cu} interaction. Next-nearest neighbor interactions are also taken into consideration. In fact, we have seen in Section IIIA that a weak antiferromagnetic interaction is acting between the copper ions in La_2Cu_3 . Consequently, we may assume a similar Cu{Cu} interaction to be present in L_2Cu_3 for $L = Tb$ and Dy . We shall denote by J^0 the Cu{Cu} interaction. Similarly, we have also taken into account a weak antiferromagnetic coupling J''^0 acting between the L ions, as suggested by the susceptibility data for Gd_2Zn_3 (Section IIIA). According to our notation, a positive coupling constant implies a ferromagnetic coupling. The presence of next-nearest neighbor interactions in 1D molecular systems based on

lanthanide ions is not new and several examples can be found in the literature.³⁴ For the case of Tb_2Cu_3 , the crystal field energy separation of the two lowest singlets of the non-Kramers Tb ion has also been included in the calculation.

To improve the reliability of the fits for Tb_2Cu_3 and Dy_2Cu_3 , we independently use the model in La_2Cu_3 to get the estimate of J^0 , and in Tb_2Zn_3 and Dy_2Zn_3 to get the estimates of J''^0 . We then fit the susceptibilities and specific heats of Tb_2Cu_3 and Dy_2Cu_3 with J^0 and J''^0 fixed at the values obtained previously with only the coupling J and the effective gyromagnetic constant g as free parameters. The fits to the susceptibility and specific heat of Tb_2Cu_3 are shown in Figs. 9 and 10, respectively. The fits provide the values of $J=k_B = 5.6$ K, $J^0=k_B = 1.0$ K, $J''^0=k_B = 1.0$ K, $\Delta = 0.2$ K and an effective gyromagnetic constant of $g = 18.0$ for the Tb ion. Similarly, the results for the susceptibility and specific heat of Dy_2Cu_3 are shown in Figs. 11 and 12, respectively. In this case, the fits provide the values of $J=k_B = 4.6$ K, $J^0=k_B = 1.0$ K, $J''^0=k_B = 1.0$ K, and effective $g = 19.6$. It can be seen that the experimental behaviors above the 3D ordering temperatures are satisfactorily reproduced. Only the specific heat of Tb_2Cu_3 is not so well accounted for (Fig. 10). Probably, this comes from the influence of low-lying excited levels, making the Hamiltonian of this system less Ising-like than for Dy_2Cu_3 . Moreover, the large g values found for both systems imply large magnetic moments which are moreover coupled ferromagnetically into chains, so that dipolar interactions may be strong enough to contribute also above the 3D ordering temperatures. Consequently, the model here presented may fail to give a detailed explanation in this temperature region. Nevertheless, the following conclusions can be drawn. The compounds Tb_2Cu_3 and Dy_2Cu_3 are very similar in behavior and are strongly anisotropic. We note that large g values of order 20, found for both Tb_2Cu_3 and Dy_2Cu_3 , have been also reported for other Dy and Tb based compounds.³⁵ For both cases, the L{Cu} interaction is predominant and ferromagnetic. This interaction is slightly stronger for Tb_2Cu_3 than for Dy_2Cu_3 , in line with the analysis reported in Ref.¹⁸. Consequently, also the 3D ordering temperature is higher for Tb_2Cu_3 ($T_C = 0.81$ K) than for Dy_2Cu_3 ($T_C = 0.75$ K). For both compounds, the presence of next-nearest neighbor interactions have to be taken into account. These interactions are much weaker than the L{Cu} interaction and are antiferromagnetic in nature. In conclusion, the results here obtained suggest that Tb_2Cu_3 and Dy_2Cu_3 order ferromagnetically within the ladders. This ordering process is accompanied by weak dipolar and probably antiferromagnetic interladder interactions, that, together with strong crystal field effects, lower the susceptibility below T_C .

For Ho_2Cu_3 , we have already reported that the Ho{Cu} interaction has to be very weak. Indeed, crystal field effects and dipolar interactions are mainly responsible for the magnetic properties at low temperature (Sec-

tion IV E). Consequently, also the 3D ordering temperature is the lowest one in comparison with Tb_2Cu_3 and Dy_2Cu_3 .

The results obtained for the magnetic interaction parameters are summarized in Table II for the Cu containing compounds and in Table III for the Zn containing compounds.

VI. CONCLUDING REMARKS

In the previous sections we have focused attention on the physical properties of spin-ladder molecular magnets containing lanthanide and transition metal ions. Together with the originality of their crystal structure, the L_2M_3 compounds present interesting magnetic features such as the onset of long-range orderings for $L = Gd, Tb, Dy, Ho$ and $M = Cu$. To the best of our knowledge, Gd_2Cu_3 is the lanthanide and transition metal ions based ferromagnet with the highest long-range ordering critical temperature $T_C = (1.78 \pm 0.02)$ K so far reported. Moreover, as estimated from specific heat and susceptibility measurements, Tb_2Cu_3 has a magnetic ordering temperature of $T_C = (0.81 \pm 0.01)$ K, while Dy_2Cu_3 orders at $T_C = (0.75 \pm 0.01)$ K, and Ho_2Cu_3 has a T_C between 0.04 and 0.10 K. These molecular based magnets are the first ones obtained with lanthanide ions other than gadolinium.

The very pronounced quasi-one-dimensionality of the magnetic structure implies that the 3D ordering is driven by the dipolar interaction acting between ladders together with the intraladder superexchange interaction. We have also reported that the intraladder $L\{Cu$ interaction is the dominant one and it is ferromagnetic for $L = Gd, Tb$ and Dy . The influence on the magnetic properties of the weaker antiferromagnetic next-nearest neighbor $L\{L$ and $Cu\{Cu$ interactions have also been analyzed. A remarkable point is the key role of the copper ions in these complex systems. They transmit the magnetic exchange interaction between the L ions across the

ladder. As a proof of this, we have seen that, if Cu is substituted by the non-magnetic Zn, the $L\{L$ interaction is inhibited and the critical temperature of the 3D ordering process is strongly diminished. Finally, the effects on the susceptibility and specific heat of the crystal field splittings of the magnetic energy levels of the lanthanide ions in L_2M_3 have been discussed and rationalized, assuming the same symmetry and coordination for the lanthanide ion in each compound of the series.

APPENDIX: ISING MODEL FOR QUANTUM SPIN LADDER

The model here reported has been developed to explain the magnetic and thermal properties of the Tb_2Cu_3 and Dy_2Cu_3 compounds.

As a first step, we assume only a coupling between the next-nearest copper (Cu) and lanthanide ($L = Tb, Dy$) ions which is ferromagnetic (in the following notations, this means $J > 0$).

For Tb and Dy, we assume an effective low-temperature spin $1/2$ and Ising coupling due to the crystal field anisotropy of the lanthanide ion. For Cu, we assume spin $1/2$ as well. The effective Hamiltonian is then:

$$H = \sum_{\langle i,j \rangle} J_{ij} (S_i S_j) + \sum_{i=1}^N g_B B_z S_i + \sum_{j=1}^N g_S B_z S_j H_z; \quad (6.1)$$

where S_i and S_j are the projections along the z axis of the spins of the copper and lanthanide ions, respectively (Fig. 15). The Landé factor of the copper ions is assumed to be $g = 2$, while the one of the lanthanide ions is a fitting parameter. The Zeeman terms in Eq. (6.1) extend over all N copper and N_S lanthanide ions.

We build the transfer matrix on the unit cell

$$T(S_1; S_2; S_1^0; S_2^0) = \sum_{i_1 i_2 i_3 i_4} \exp \left[J_{11} (S_1 + S_1^0) + J_{22} (S_2 + S_2^0) + \frac{1}{2} J_{33} (S_1 + S_2^0) + \frac{1}{2} J_{44} (S_1 + S_2^0) \right. \\ \left. + \frac{1}{2} g_S B_z H_z (S_1 + S_1^0 + S_2 + S_2^0) + g_B B_z H_z \left(\frac{1}{2} + \frac{1}{2} + \frac{1}{2} J_{33} + \frac{1}{2} J_{44} \right) \right]$$

where $\beta = 1/k_B T$. The partition is expressed in terms of the 4×4 transfer matrix

$$Z(T; H_z) = \sum_{S_1} T(S_1; S_2; S_1^0; S_2^0) T(S_1^0; S_2^0; S_1^0; S_2^0) \dots$$

$$\lim_{N \rightarrow \infty} \frac{1}{N} \ln Z = \ln \lambda_{\max}$$

Therefore, by defining

$$\lambda_{\max} = \lim_{N \rightarrow \infty} \frac{1}{N} \ln Z = \ln \lambda_{\max}$$

where λ_{\max} is the largest eigenvalue of T , we obtain numerically

ically the magnetic susceptibility and the molar specific heat by

$$= k_B T \frac{\partial^2 f}{\partial H_z^2} \quad ; \quad C = k_B^2 \frac{\partial^2 f}{\partial T^2} :$$

According to the susceptibility data of La_2Cu_3 (Fig. 2), we assume a slight antiferromagnetic next-nearest neighbor coupling J^0 between the copper ions. Similarly, ac-

cording to the susceptibility data of Gd_2Zn_3 (Fig. 2), we expect an antiferromagnetic next-nearest neighbor coupling J^0 between the lanthanide ions. In both cases, the data are compatible with couplings not exceeding 1 K. By adding these second neighbors couplings we get the complete scheme depicted in Figure 15.

The transfer matrix is now

$$\begin{aligned} T(S_1; S_3; S_2; S_1^0; S_4; S_2^0) = & \sum_{S_1; S_2} \exp \left[J_{11}(S_1 + S_1^0) + J_{22}(S_2 + S_2^0) + \frac{1}{2} J_{33}(S_1 + S_2^0) + \frac{1}{2} J_{44}(S_1 + S_2^0) \right. \\ & \left. \exp \left[J^0(S_1 + S_2)(S_3 + S_4) + J^0 S_1 S_1^0 + S_2 S_2^0 + \frac{1}{2} (S_1 S_2 + S_1^0 S_2^0) \right] \right. \\ & \left. \exp \left[\frac{1}{2} g_B H_z (S_1 + S_1^0 + S_2 + S_2^0) + g_B H_z (S_3 + S_4) + \frac{1}{2} J_{33} + \frac{1}{2} J_{44} \right] \right] \end{aligned}$$

with $J > 0$, $J^0 < 0$ and $J^0 < 0$. This is now an 8 × 8 matrix but the process is the same.

For the terbium case, that is a non-Kramers ion, we allow the spin states to be non degenerate by adding to the Hamiltonian a term $E(S_i)$ such that $E(+\frac{1}{2}) = \frac{1}{2}$ and $E(-\frac{1}{2}) = -\frac{1}{2}$, where $\frac{1}{2}$ is the gap. The best fits for Tb_2Cu_3 are displayed in Figs. 9, 10 and for Dy_2Cu_3 in Figs. 11, 12.

ACKNOWLEDGMENTS

We are indebted to F.L. Mettes, F. Luis, A. Morello, and D. Culbra for the low-temperature experiments. This work was partially supported by Grant No. MAT 99/1142 from CICYT.

* Present address: Kamerlingh Onnes Laboratory, Leiden University, 2300 RA, Leiden, The Netherlands. Electronic mail: evange@phys.leidenuniv.nl.

[†] Present address: Laboratoire de Chimie de Coordination, UPR CNRS 8241, 31077 Toulouse, France.

¹ see, for instance, D. Gatteschi, *Adv. Mater.* **6**, 635 (1994) and references therein.

² O. Kahn, *Molecular Magnetism*, (VCH, New York, 1993).

³ O. Kahn, *Angew. Chem., Int. Ed. Engl.* **24**, 834 (1985).

⁴ for a recent review on molecular materials with lanthanide ions, see C. Benelli and D. Gatteschi, *Chem. Rev.* **102**, 2369 (2002) and references therein.

⁵ A. Bencini, C. Benelli, A. Caneschi, R.L. Carlin, A. Dei, and D. Gatteschi, *J. Am. Chem. Soc.* **107**, 8128 (1985).

⁶ A. Bencini, C. Benelli, A. Caneschi, A. Dei, and D. Gatteschi, *Inorg. Chem.* **25**, 572 (1986).

⁷ C. Benelli, A. Caneschi, D. Gatteschi, O. Guillou, and L. Pardi, *Inorg. Chem.* **29**, 1750 (1990).

⁸ M. Sakamoto, M. Hashimura, K. Matsuki, N. Matsumoto, K. Inoue, and H. Okawa, *Bull. Chem. Soc. Jpn.* **64**, 3639 (1991).

⁹ J.P. Costes, F. Dahan, A. Dupuis, and J.P. Laurent, *Inorg. Chem.* **35**, 2400 (1996).

¹⁰ I. Ramade, O. Kahn, Y. Jeannin, and F. Robert, *Inorg. Chem.* **36**, 930 (1997).

¹¹ J.P. Costes, F. Dahan, A. Dupuis, and J.P. Laurent, *Inorg. Chem.* **36**, 3429 (1997).

¹² M. Andruh, I. Ramade, E. Codjovi, O. Guillou, O. Kahn, and J.C. Trombe, *J. Am. Chem. Soc.* **115**, 1822 (1993).

¹³ O. Kahn and O. Guillou in *Research Frontiers in Magnetochemistry*, C.J.O'Connors (Ed.), (World Scientific, Singapore, 1993).

¹⁴ R. Georges, O. Kahn, and O. Guillou, *Phys. Rev. B* **49**, 3235 (1994).

¹⁵ F. Bartolome, J. Bartolome, R.L. Oushoom, O. Guillou, and O. Kahn, *J. Magn. Magn. Mater.* **140-144**, 1711 (1995).

¹⁶ M. Evangelisti, F. Bartolome, J. Bartolome, M.L. Kahn, and O. Kahn, *J. Magn. Magn. Mater.* **196-197**, 584 (1999).

¹⁷ J.F. Herbst, *Rev. Mod. Phys.* **63**, 819 (1991) and references therein.

¹⁸ M.L. Kahn, C. Mathoniere, and O. Kahn, *Inorg. Chem.* **38**, 3692 (1999).

¹⁹ M. Evangelisti, J. Bartolome, F. Mettes, L.J. de Jongh, M.L. Kahn, C. Mathoniere, and O. Kahn, *Polyhedron* **20**, 1447 (2001).

²⁰ M. Azuma, Z. Hiroi, M. Tanaka, K. Ishida, and I. Kitaoka, *Phys. Rev. Lett.* **73**, 3463 (1994).

²¹ T. Barnes and J. Riera, *Phys. Rev. B* **49**, 6817 (1994).

²² Z. Hiroi and M. Takano, *Nature* **377**, 41 (1995).

- ²³ for a recent review on molecular spin ladders, see C. Rovira, Chem. Eur. J. 6, 1723 (2000) and references therein.
- ²⁴ R.L. Oushoom, K. Boubekeur, P. Batail, O. Guillou, and O. Kahn, Bull. Soc. Chim. Fr. 133, 777 (1996).
- ²⁵ M.L. Kahn, M. Verelst, P. Lecante, C. Mathoniere, and O. Kahn, Eur. J. Inorg. Chem., 527 (1999).
- ²⁶ M. Verelst, L. Sommer, P. Lecante, A. Mosset, and O. Kahn, Chem. Mater. 10, 980 (1998).
- ²⁷ A. van der Bilt, K.O. Joung, R. Carlin, and L.J. de Jongh, Phys. Rev. B 22, 1259 (1980).
- ²⁸ J. Bartolome and F. Bartolome, Phase Trans. 64, 57 (1997).
- ²⁹ Considering the simple case of isotropic interaction with no anisotropy term but with a magnetic field added, $H = J \sum_{i,j} S_i^z S_j^z - g_B \mu_B \sum_i S_i^z H$, the mean field expression for the Curie-Weiss temperature is thus given by $k_B T_C = \frac{1}{3} z J S(S+1)$, where z is the number of neighboring spins.
- ³⁰ K.R. Lea, M.J.M. Leask, and W.P. Wolf, J. Phys. Chem. Solids 23, 1381 (1962).
- ³¹ L.J. de Jongh and A.R. Miedema, Adv. Phys. 50, 947 (2001).
- ³² O. Guillou, P. Bergerat, O. Kahn, E. Bakalbassis, K. Boubekeur, P. Batail, and M. Guillot, Inorg. Chem. 31, 110 (1992).
- ³³ see, for instance, A. Abragam and B. Bleaney, Electron paramagnetic resonance of transition ions, (Oxford University Press, London, 1970).
- ³⁴ D. Gatteschi, A. Caneschi, and R. Sessoli in Molecular Magnetism: From Molecular Assemblies to the Devices, E. Coronado et al. (Eds.), (Kluwer Academic Publishers, Dordrecht, 1996) and references therein.
- ³⁵ see, for instance, R.L. Carlin, Magnetochemistry, (Springer-Verlag, Berlin, 1986), pag. 252, and references therein.

	Gd ₂ Cu ₃	Tb ₂ Cu ₃	Dy ₂ Cu ₃	Ho ₂ Cu ₃	Gd ₂ Zn ₃	Ho ₂ Zn ₃
	3.2	1.5	8.8	1.2	1.1	2.9

TABLE I: Experimental lattice contributions ($C_1 = R = T^3$) as estimated from the data in Fig. 4. The values are expressed in ($10^{-2} K^{-3}$).

	La ₂ Cu ₃	Gd ₂ Cu ₃	Tb ₂ Cu ₃	Dy ₂ Cu ₃	Ho ₂ Cu ₃
T_C (K)		1.78(2)	0.81(1)	0.75(1)	0.04 0.10
(K)	0.2	2.3			
$J = k_B$ (K)		0.74	5.6	4.6	
$J^0 = k_B$ (K)	0.2		1.0	1.0	
$J^{00} = k_B$ (K)			1.0	1.0	
(K)			0.2 (s{s)		1.1 (d{t)
g_L		2	18.0	19.6	
Model	MF	Georges	App.	App.	Schottky-LLW

TABLE II: Experimental results obtained for the Cu containing compounds. T_C is the long-range magnetic ordering temperature; J is obtained from the Curie-Weiss law (Section III); J , J^0 and J^{00} are the exchange constants for the L{Cu, Cu{Cu and L{L interactions, respectively (negative values stand for antiferromagnetic interactions); Δ is the separation between the ground state and the first excited state (included also is the type of state: s= singlet; d= doublet; t= triplet); g_L is the Lande factor for the L ion; the models used are MF (mean field) or LLW (Section IIIB) or Georges (Section V A) or App. (Appendix and Section V B) or Schottky (Section IV E).

	Gd ₂ Zn ₃	Tb ₂ Zn ₃	Dy ₂ Zn ₃	Ho ₂ Zn ₃
(K)	0.1			
$J^{00} = k_B$ (K)	6 10 ⁻³	1.0		
(K)		0.2 (s{s)	13.7 (d{d)	8.3 (d{t)
Model	MF	LLW-App.	LLW	LLW

TABLE III: Experimental results obtained for the Zn containing compounds. The same notation of Table II is used.

LIST OF FIGURES

1. Relative dispositions of the ladders: (a) view of two neighboring ladders in the bc plane; (b) schematic view of the ladders projected in the ac plane. The lanthanide ions are located on the sides of the ladder and occupy each corner, while each transition metal ion is between two lanthanide ions along the sides and in the rungs.
2. TOP: Experimental molar susceptibility of La_2Cu_3 . In the inset: the same data plotted as χ^{-1} vs T . BOTTOM: Inverse of the in-phase susceptibilities of Gd_2Zn_3 () and GdCu_3 (). In the inset: χ^{-1} vs T for Gd_2Zn_3 .
3. TOP: Experimental inverse susceptibility for Tb_2Zn_3 . The solid line is the calculated inverse susceptibility taking into account $\theta = 0.2$ K and $J^0_{\text{B}} = 1$ K for the $\text{Tb}\{\text{Tb}\}$ interaction. For explanations, see text. CENTER: Measured and calculated inverse susceptibility for Dy_2Zn_3 . BOTTOM: Measured and calculated inverse susceptibility for Ho_2Zn_3 .
4. Experimental specific heats of LaM_3 .
5. Experimental molar in-phase susceptibility of Gd_2Cu_3 versus temperature and theoretical estimation for $J = k_B = 0.74$ K (see Section V A for explanations).
6. Field dependence of the magnetization and hysteresis loop at $T = 1.70$ K for Gd_2Cu_3 . The dotted line represents the Brillouin functions as calculated from Eq. (4.1).
7. Magnetic specific heat vs temperature for Gd_2Zn_3 . Solid curve is a guide to the eye.
8. Magnetic molar specific heat vs temperature for Gd_2Cu_3 . Curve a is the ferromagnetic spin wave contribution ($\propto T^{3/2}$); curve b is the high temperature limit ($\propto T^2$) of the magnetic anomaly tail. In the inset: temperature dependence of the magnetic entropy for Gd_2Cu_3 .
9. Experimental low-temperature in-phase susceptibility vs temperature for Tb_2Cu_3 together with the calculated susceptibility (for explanations see Section V B). In the inset: Experimental out-of-phase susceptibility.
10. Magnetic molar specific heat of Tb_2Cu_3 . The dotted line is the calculated hyperfine contribution of the Tb ions. The solid line is the calculated specific heat due to the low-dimensionality of the ladder (for explanations see Section V B).
11. Experimental low-temperature in-phase susceptibility vs temperature for Dy_2Cu_3 together with the calculated susceptibility (for explanations see Section V B). In the inset: Experimental out-of-phase susceptibility.
12. Magnetic molar specific heat of Dy_2Cu_3 . The solid line is the calculated specific heat due to the low-dimensionality of the ladder (for explanations see Section V B).
13. Experimental molar in-phase and out-of-phase (inset) susceptibilities vs temperature for Ho_2Cu_3 . Solid curves are guides to the eye.
14. Magnetic molar specific heat of Ho_2Cu_3 () and Ho_2Zn_3 (). The solid line is the calculated Schottky contribution due to the splitting of the $^{(2)}_3$ and $^{(2)}_4$ levels of the holmium ions as shown in the Figure. In the inset the same data in log-log scale.
15. Ladder structure considered by the model discussed in the Appendix.

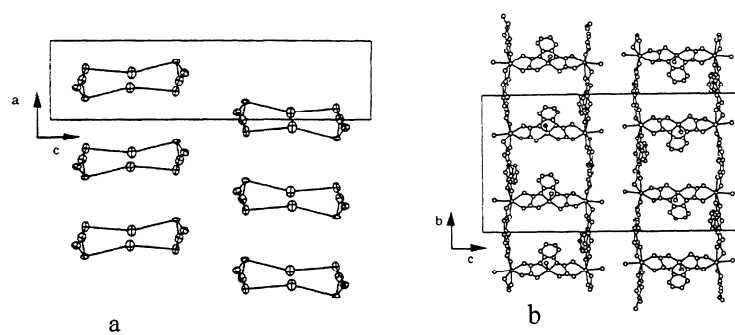


Fig. 1, M. Evangelisti et al., PRB

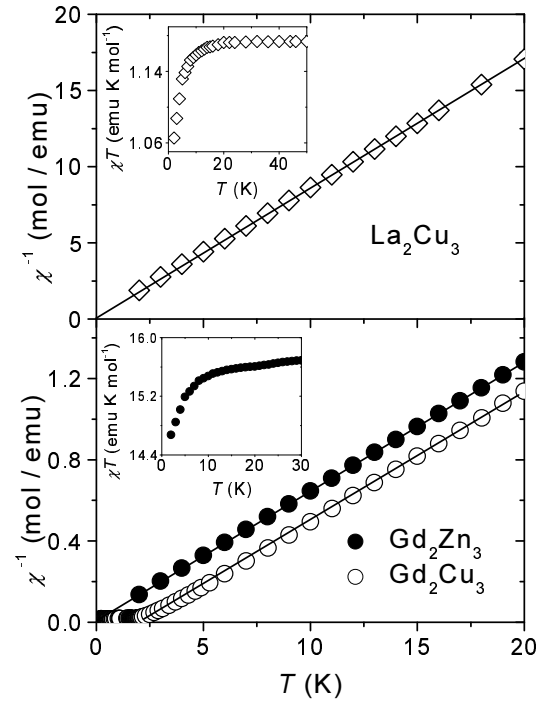


Fig. 2, M. Evangelisti et al., PRB

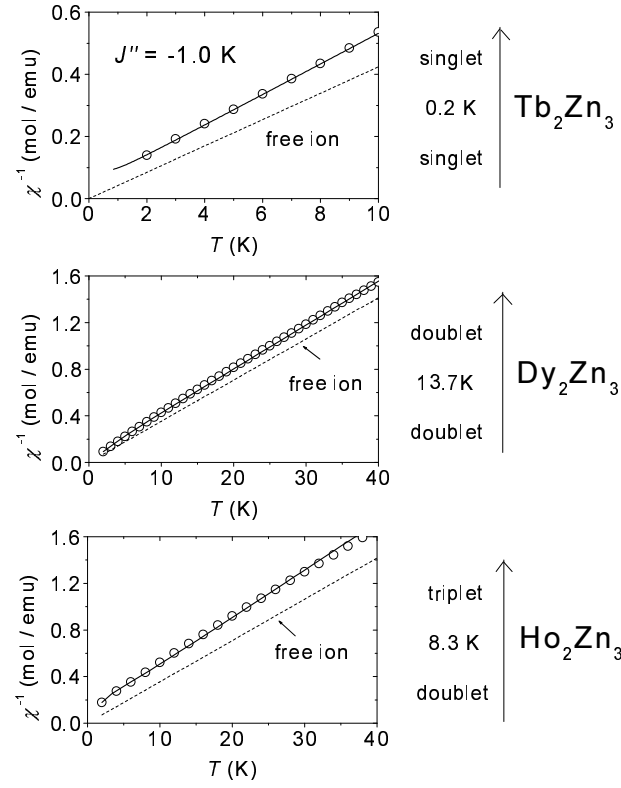


Fig. 3, M. Evangelisti et al., PRB

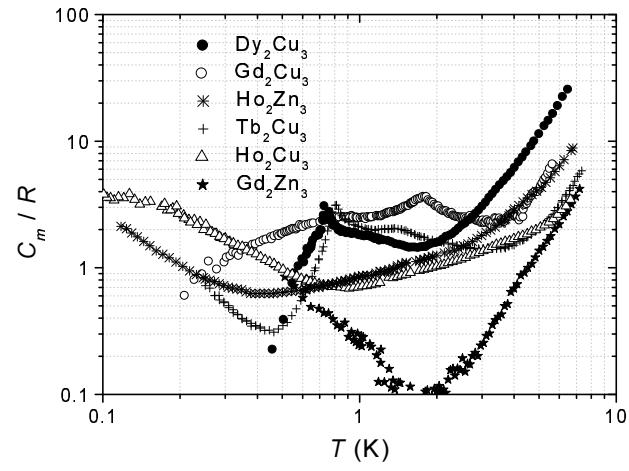


Fig. 4, M. Evangelisti et al., PRB

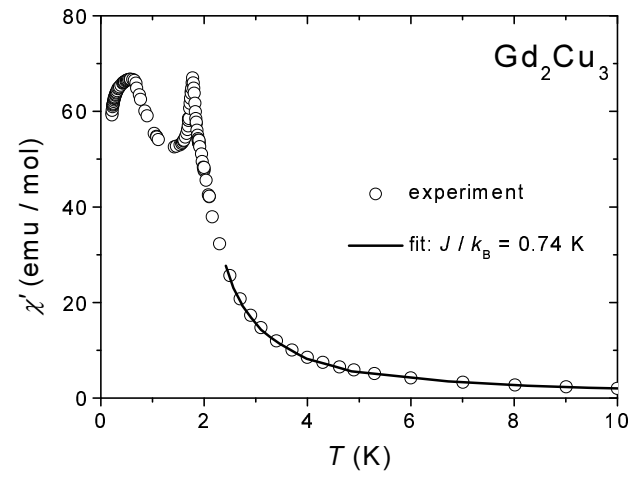


Fig. 5, M. Evangelisti et al., PRB

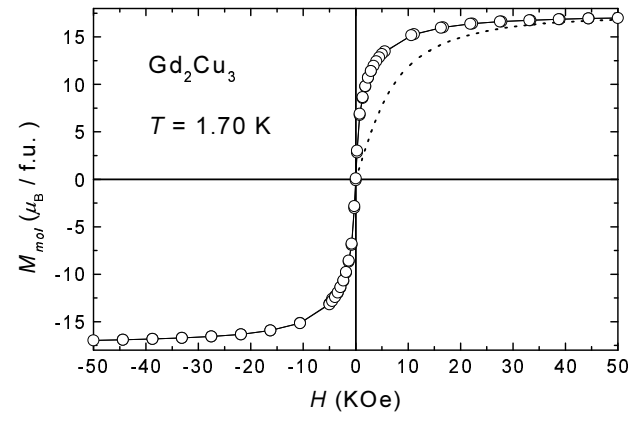


Fig. 6, M. Evangelisti et al., PRB

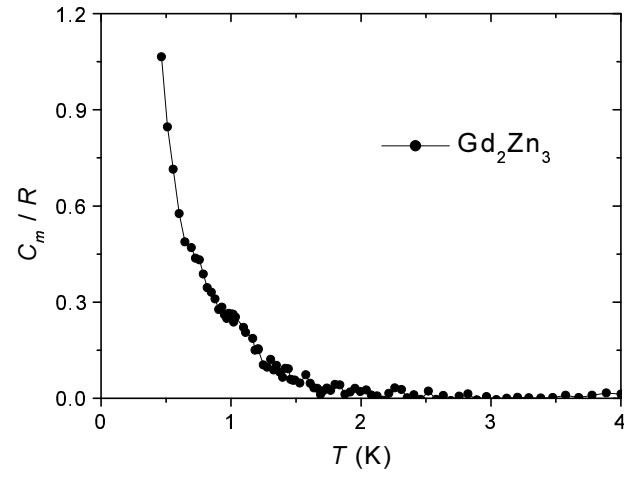


Fig. 7, M. Evangelisti et al., PRB

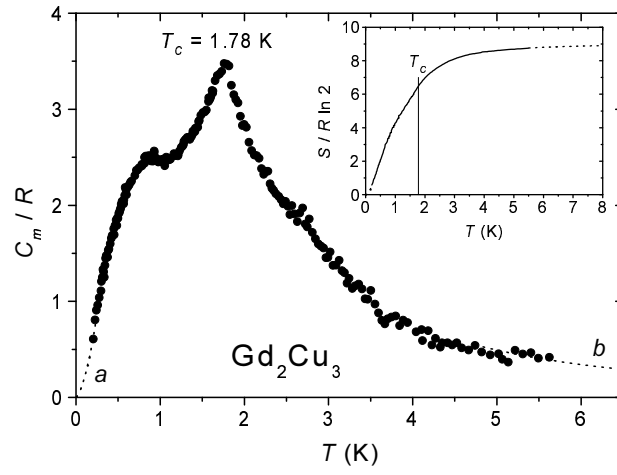


Fig. 8, M. Evangelisti et al., PRB

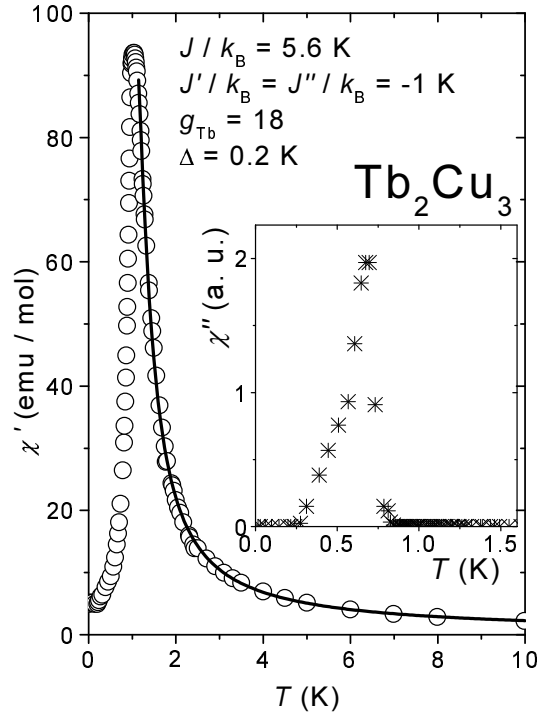


Fig. 9, M. Evangelisti et al., PRB

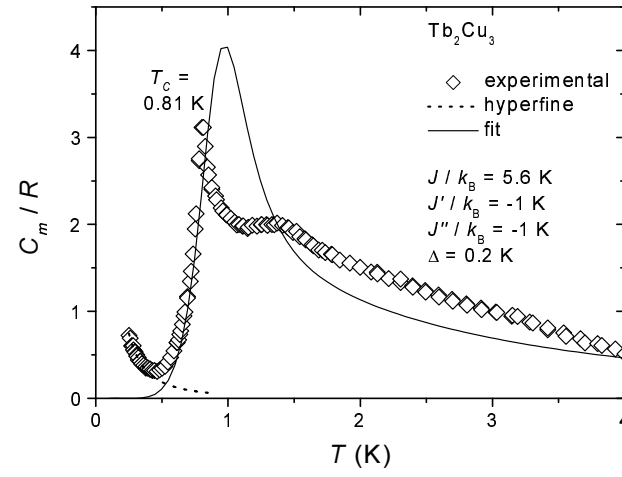


Fig. 10, M. Evangelisti et al., PRB

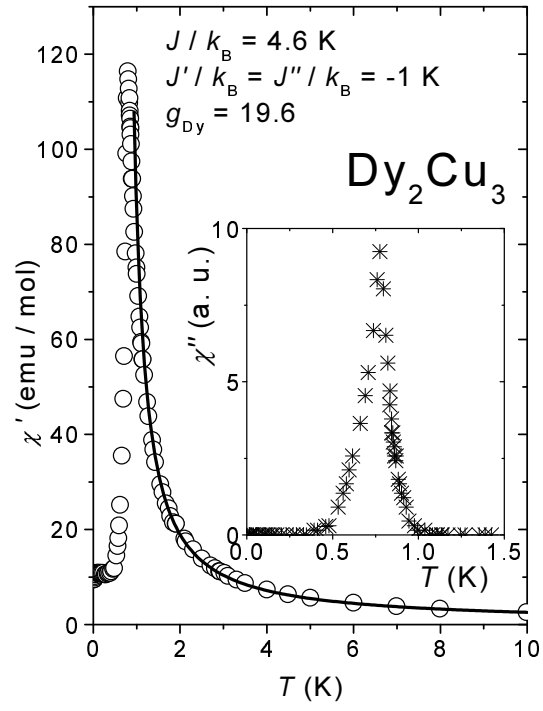


Fig. 11, M. Evangelisti et al., PRB

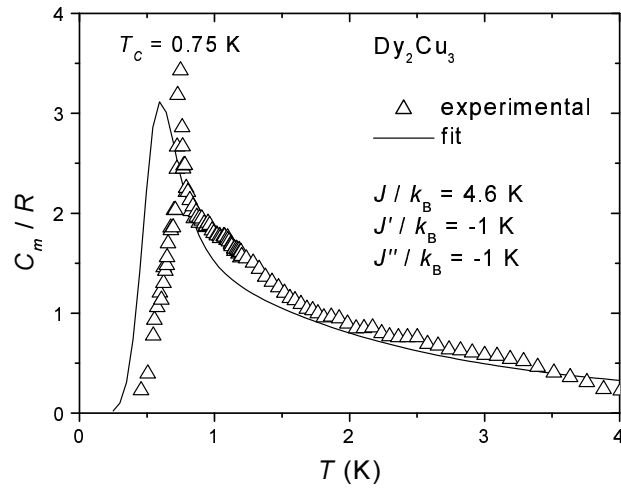


Fig. 12, M. Evangelisti et al., PRB

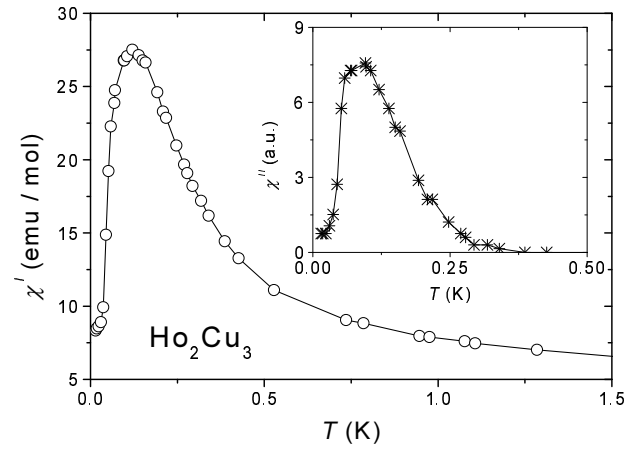


Fig. 13, M. Evangelisti et al., PRB

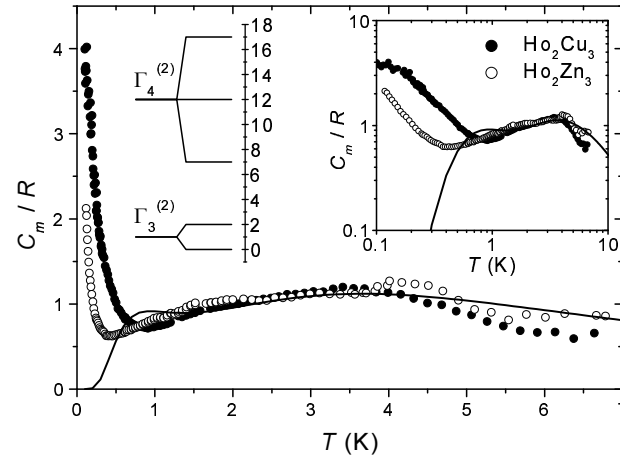


Fig. 14, M. Evangelisti et al., PRB

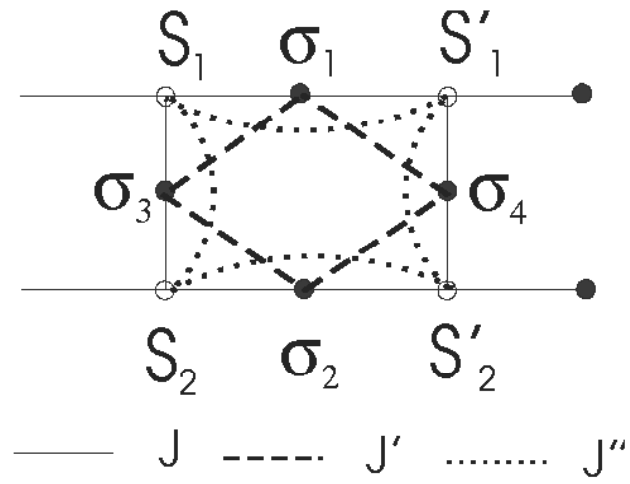


Fig. 15, M. Evangelisti et al., PRB